Theoretical optimization and prediction in the experimental search space for vibrational quantum processes

C. Gollub[1,*] and R. de Vivie-Riedle[1,†]
[1]*LMU Department Chemie, Butenandt-Strasse 11, 81377 München, Germany*
(Received 14 July 2008; published 22 September 2008)

Control and optimization prospects in the frequency domain are studied theoretically, using a genetic algorithm (GA) and shaping Fourier-limited (FL) pulses. The objectives are state-to-state transitions and unitary transformations, within the scope of vibrational excitation of transition metal carbonyls. In analogy to experimental closed-loop setups, two different implementations of the phase function are investigated: a free phase variation and a sinusoidal phase modulation. We examine the control landscape generated by the parametrized phase functions and clarify the underlying mechanism. Strategies to decrease the complexity of the laser fields are developed, benefiting from previous optimal control theory calculations. Additionally, we pass the capabilities of the experiment and optimize the FL pulses with the GA simultaneously to the phase and transmittance functions. This allows us to predict promising FL-pulse properties and mask functions for future experiments.

DOI: 10.1103/PhysRevA.78.033424 PACS number(s): 32.80.Qk, 33.80.−b, 33.20.Ea, 02.30.Yy

I. INTRODUCTION

Optimal control theory (OCT) [1–3] and optimal control experiments (OCE) [4,5] have been successfully demonstrated for numerous applications in molecular physics, driving control processes with modulated laser pulses. However, the underlying search strategies differ; while OCT operates in the time domain, OCE optimizes the laser fields in the frequency domain. This implies that both search procedures experience a different bias and follow different pathways on the search landscape. A clear advantage of OCT is the possibility to strictly limit the molecular laser interaction time, which is important, especially in the condensed phase, where decoherence sets an upper limit for the temporal control window. In the parameter space of OCT it was possible for different examples [6,7] to find a subspace of high-fidelity solutions with simple structured laser fields providing robust mechanisms.

Now the question arises, whether and how OCE solutions can be traced in the OCT domain. We explore the possible overlap of OCE and OCT subspaces and whether OCT solutions can be approached in an OCE search, based on genetic algorithms (GA) for amplitude and phase modulation.

Shaped laser fields are obtained by applying phase and transmittance functions on FL pulses. The pulse shapers are either liquid crystal spatial light modulators or acousto-optical modulators. In close analogy to the experiment, we perform the optimization of the laser fields with GAs starting from ultrashort FL pulses. The phase functions are either optimized on the pixel basis, or specified as analytic functions. We explore the search space and strategy of GAs in relation to OCT solutions. As an example, we select carbonyl complexes, whose controllability with shaped pulses are already studied [8–10] to some extent. The objectives are state-to-state transitions and unitary transformations for the two metal carbonyls $W(CO)_6$ and $MnBr(CO)_5$. In the theoretical simulation, the experimental constraints, e.g., the incident pulse duration, the carrier frequency, the maximum energy, and the properties of the mask functions, can be met and conserved in the beginning and during the optimization. The principle possibility to optimize quantum gates with GAs theoretically, has been demonstrated previously [11,12] for small molecules.

In this study, we focus on similarities and differences of GA and OCT searches and solutions found. Based on our knowledge from previous OCT control studies, we aim for simple and robust GA solutions. This allows for the prediction of a promising and concerted search strategy and for optimal solutions within the control space of the experiment.

II. MODEL SYSTEMS AND COMPUTATIONAL DETAILS

The control studies are performed for CO-stretching normal modes of the metal carbonyls $W(CO)_6$ and $MnBr(CO)_5$. The potential energy curve of the T_{1u} mode of $W(CO)_6$ and the corresponding dipole moment are calculated quantum chemically [13] with density functional theory (b3lyp/6-31G*, LANL2DZ for W); in the case of $MnBr(CO)_5$ see [9]. The vibrational eigenfunctions are explicitly calculated by a relaxation method [14], the dipole matrix elements are evaluated, and the Hamiltonian is set up in the eigenstate representation. In the case of the molecule $W(CO)_6$, we use the vibrational eigenstates from the transient spectrum [8] to simulate the experimental conditions accurately; the energy of the higher lying vibrational levels are extrapolated with the anharmonicity traced from the spectrum. The time propagation is performed with the split-operator technique, where the wave packet is expanded in the basis of vibrational eigenstates with time-dependent complex coefficients. For the quantum gate calculations we define the vibrational ground state as the qubit state $|0\rangle$ and the first vibrational excited state as $|1\rangle$.

*Caroline.Gollub@cup.uni-muenchen.de
†Regina.de_Vivie@cup.uni-muenchen.de

III. OPTIMIZATION WITH GENETIC ALGORITHMS

OCT is established as a powerful tool for various control tasks and for the interpretation of the induced control mechanisms. An optimality criterion has to be achieved and optimal control finds an appropriate control law for it, the optimal laser field. Additionally, the control problems include ancillary constraints, such as the time-dependent Schrödinger equation. The optimal control calculations are performed in the time domain and the conditions of learning loop experiments [8,15] with bandwidth tailored pulses, cannot be introduced directly in the frequency domain, but can be simulated using frequency filters in the time domain [7]. An experimental learning loop consists of a pulse shaper, a feedback signal and an evolutionary algorithm. The same experimental parameters are used in the theoretical application of the GA. For state-to-state transitions and unitary transformations for carbonyl complexes, we explore the prospects of the GA method. The learning loop experiments are theoretically described, by sending FL pulses through a shaper and calculating the feedback signals with the knowledge of the Hamiltonian. The phase and transmittance functions are optimized by the GA to reach high efficiencies of the control processes.

The incident, bandwidth limited pulses have a Gaussian shape and are centered at the carrier frequency ω_c as follows:

$$E(t) = E_0 \exp\{-(t/\tau_G)^2\}\cos(\omega_c t) \quad \text{with } \tau_G = \tau_p/\sqrt{2\ln 2}.$$

The FL-pulse duration τ_p is the full width at half maximum (FWHM) of the intensity profile and the spectral width $\Delta\omega_p$ is the FWHM of the spectral intensity.

$$E(\omega) = E_0 \exp\left\{-2\ln 2\left(\frac{\omega-\omega_c}{\Delta\omega_p}\right)^2\right\}.$$

E_0 is the maximum intensity in each case, t is the time, and ω is the frequency. The phase $\phi(\omega)$ is set to zero for bandwidth limited pulses.

After passing the shaper with the transmittance function $T(\omega)$ and the phase function $\phi(\omega)$ the pulse is modulated according to

$$E^{\mathrm{mod}}(\omega) = E_0\sqrt{T(\omega)}\exp\left\{-2\ln 2\left(\frac{\omega-\omega_c}{\Delta\omega_p}\right)^2\right\}\exp\{i\phi(\omega)\}.$$

Both functions $T(\omega)$ and $\phi(\omega)$ are discrete, depending on the spectral resolution of the shaper, but interpolated afterwards by a cubic spline interpolation scheme.

In the case of the phase function $\phi(\omega)$ two approaches are possible; it can be either optimized in an analytic form [8] with i different parameters or each value of the phase function can be varied individually. For a shaper with N pixels, i or N parameters have to be optimized for the phase function. If additionally a transmittance function $T(\omega)$ is taken into account in similar ways, the number basically doubles and a vector consisting of all these parameters has to be optimized by the GA. The codomain of the phase function $\phi(\omega)$ is $[0,2\pi]$, whereas the transmittance is defined in the range of $[0,1]$.

We only briefly introduce the basic principle of GAs; more detailed information can be found elsewhere [16]. GAs are global search heuristics and are a class of evolutionary algorithms. They are used for combinatorial optimization problems. The basic ideas are taken from evolutionary biology such as mutation, selection, and crossover. For the first generation, a starting population of candidate solutions (called individuals) is randomly generated. Each individual has a genome, which is the phase and transmittance function used to modulate the FL pulse in our simulation. The fitness of every individual is evaluated. We propagate each generated laser field of the actual population and calculate the efficiency. Now, a tournament selection of the individuals, based on their fitness, is performed and they are randomly recombined and mutated to build a new generation, which is evolving in the next iteration. In this study, a steady-state GA from the GAlib genetic algorithm package [17] is applied, which replaces only the individuals with the lowest fitness by offsprings. As an advantage, good solutions remain in the population for more iterations.

In optimal control calculations [6,1–3], pulse parameters are entered in terms of a guess laser field, but they are not binding for the formalism and are generally altered during the optimization, except of the pulse duration. OCT-specific parameters, which need to be chosen initially, are a penalty factor for the restriction of the pulse energy and a shape function, to ensure a smooth switching on and off behavior of the pulse intensity. For the GA, one has to specify the FL-pulse parameters as well as the number of pixels and the pixel width explicitly and these parameters stay fixed during the optimization. Solutions for the selected FL-pulse and pixel properties are generated exclusively, whereas, in OCT the required properties of the FL pulses can be deduced from the optimal field [18] and can vary for runs with different penalty factors. Additional GA-specific input data are the mutation rate, the crossing-over rate, the replacement factor, the population size, and the sampling of the shaper. We use the parameters 0.33 for the replacement rate, 0.05 for the mutation rate, and 0.95 for the crossover rate.

IV. RESULTS AND DISCUSSION

We present and discuss the results for the state selective excitation of the T_{1u} of $W(CO)_6$ in analogy to the experiment presented in [8] as well as the quantum gates predicted for the metal carbonyls with sinusoidal phase functions and freely optimized phase and transmittance functions. Strategies, based on the knowledge from previous OCT calculations, are used and lead to simplifications of the resulting laser fields.

A. NOT gate: T_{1u} mode of $W(CO)_6$

Our first optimization aim is the NOT gate operation, switching the qubit basis states $|0\rangle \leftrightarrow |1\rangle$ for the qubits encoded in the vibrational ground and first excited state of a T_{1u} normal mode of $W(CO)_6$. The pixeled phase $\phi(\omega)$ and transmittance function $T(\omega)$ are optimized with a spectral pixel resolution of 10 cm^{-1}. The FL-pulse parameters are given in Table I, first row.

The best individual yields an efficiency of 99.6% and a rather complex envelope function, depicted in Fig. 1(a).

TABLE I. FL-pulse properties for NOT gates.

τ_p (fs)	E_0 (a.u.)	ω_c (cm^{-1})
105	0.002	2000
480	0.001	2000
700	0.0003	2000

Similar structures of highly efficient quantum gates have been reported earlier for different molecules [19,11,12]. For more robust laser fields, we now focus on the simplification of such pulses, in favor of adiabatic state switching and low field intensities. From OCT, we are aware of a certain tendency to longer FL pulses for gate operations in the carbonyl complexes. We increase the FWHM of the FL pulse and use the parameters given in Table I, second row. A clear simplification of the envelope function results with a shorter time duration and only of a few subpulses [Fig. 1(b)]. In our previous OCT work [20] the variation of the phase functions was very small. Thus we assume that the envelope functions can further be simplified, when additionally the maximum phase variation is limited, i.e., the codomain is decreased from $[0,2\pi]$ to $[0,2\pi]\times 0.1$. The result is shown in Fig. 1(c), upper panel, in the time domain and in the lower panel, in the frequency domain. The envelope reveals three subpulses, which might be interpreted as a multipulselike structure.

For comparison, a corresponding OCT calculation was performed, where we used a total pulse duration of 5.3 ps for the shaped OCT pulse and a penalty factor $\alpha=200$. The resulting, highly efficient NOT gate laser field (99.3%) is presented in Fig. 1(e), together with the calculated spectrum (dashed, black line) and mask functions [phase: solid, gray line; transmittance: solid, black line; both not interpolated, spectral pixel width <7 cm^{-1}, lower panel of Fig. 1(e)]. The field is almost completely amplitude modulated, but not phase shaped. The FWHM of the corresponding FL pulse is elongated to 825 fs and the spectrum is centered at the fundamental transition frequency.

We now use the FL pulse derived from the OCT result for GA calculations and use a spectral pixel width of 6 cm^{-1}. First, we confine the codomain of the phase function to a minimum range of $[0,2\pi]\times 0.01$. The resulting NOT gate (not shown here) is also highly efficient, however, the phase is still varying and the GA fully uses the available range the phase function is limited to. Statistically, varying phases are much more probable than constant phase functions in GA

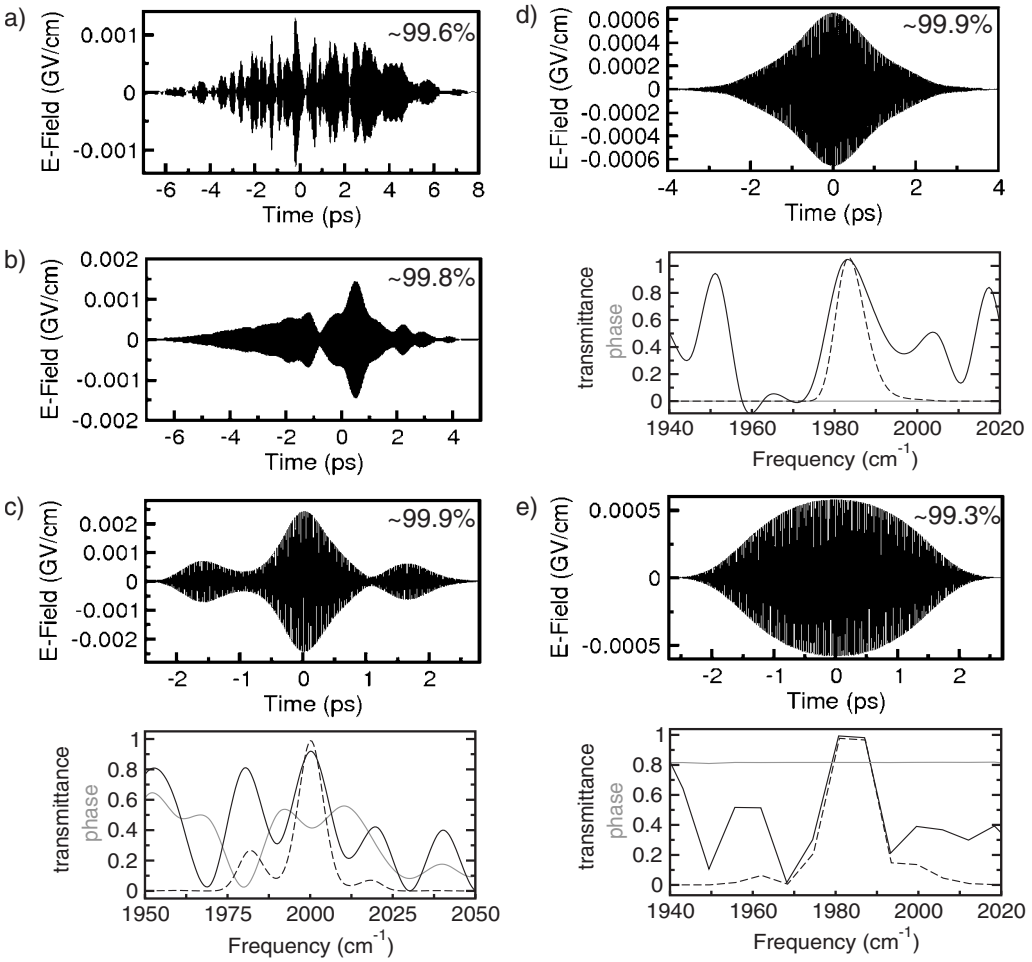

FIG. 1. (a) , (b) and upper panels of (c), (d):NOT gates optimized with a GA. Lower panels: spectra (scaled, dashed, black line), phase (gray line), and transmittance (solid, black line) functions. Due to the cubic spline interpolation the transmittance might slightly overshoot the range [0, 1]; this should not affect the validity of the results. (e) OCT result for the NOT gate.

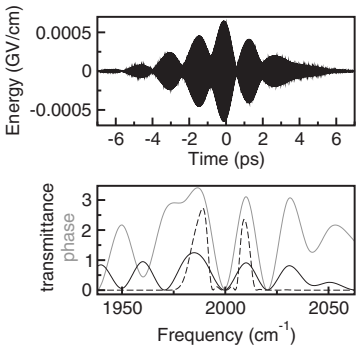

FIG. 2. Upper panel: Hadamard gate; lower panel: spectrum (dashed, black line), phase function $\phi(\omega)$ (gray line), and the transmittance function $T(\omega)$ (solid, black line).

optimizations. As these phases already give good solutions, the GA has no bias for flat phase functions. No correlation is imposed on the phase values of the pixels to enforce constant phase functions, as in the case of OCT, where this is indirectly implemented by the use of high penalty factors α. Thus, the OCT optimization explores and converges in a different part of the search space compared to theoretical and experimental GA applications. Ultimately, we allow only amplitude shaping of the OCT-FL pulse in the GA and the resulting field is shown in Fig. 1(d). An efficiency exceeding 99.9% is reached, and the GA finds a solution very close to the OCT result. The main difference is in the duration, as the GA offers no time constraint for the optimized pulse [Figs. 1(d) and 1(e), upper panels]. Although limitations on the phase range lead to simplified control fields, more demanding control tasks will require some flexibility in the phase function [20].

The strategy of elongated FL pulses and a limited codomain of the phase function, is also tried for a Hadamard operation. A spectral pixel resolution of 10 cm^{-1} is used and the parameters for the FL pulse are given in Table I, third row. For high quantum yield the boundaries for the phase variation must be relaxed to $[0,2\pi]\times 0.5$ and efficiencies exceeding 99.4% are received (Fig. 2).

B. Constraints in the objective function

Purely pixel-based GA optimizations yield complex field structures for unitary transformations. Simplifications of pulse structures can be achieved, when the knowledge from OCT results is used, i.e., simple solutions can be found within the search space of the GA. As OCT results are not always available, a favorable alternative is the implementation of constraints in the GA approach, in analogy to OCT. In Sec. IV A, the objective was simply defined by the efficiency of the population transfer as follows:

TABLE II. FL-pulse properties for a constrained search.

τ_p (fs)	E_0 (a.u.)	ω_c (cm^{-1})
725	0.001	2000

$$O = \frac{1}{N}\sum_{k=1}^{N} |\langle \Psi_{ik}(T)|\Phi_{fk}\rangle|^2,$$

with each of the k wave functions $\Psi_i(T)$ propagated to the final time T and the target states Φ_f. We can now subtract the field intensity weighted by a penalty factor α from the overlap term as follows:

$$O = \frac{1}{N}\sum_{k=1}^{N} |\langle \Psi_{ik}(T)|\Phi_{fk}\rangle|^2 - \alpha\int_0^T E(t)^2 dt.$$

Consequently, efficient laser fields with low intensities dominate the ones with high intensities.

For a mask function with a spectral pixel resolution of 10 cm^{-1} and the FL-pulse parameters given in Table II, we scanned the penalty factor α exemplarily for the state-to-state transition $0\rightarrow 1$ (Fig. 3). α is given in units of $bohr^2$/hartree, when used as penalty factor for the pulse energy. Accordingly with ascending values of α, the maximum objective reached decreases and the monotonic convergence of the GA runs slightly vanishes (Fig. 3, left). Still, control efficiencies above 99% are reached up to a value of $\alpha=20$ and the monotonic convergence stays mostly acceptable. The resulting envelope functions (Fig. 3, right) more and more resemble each other with increasing α and we can deduce that the GA is guided towards similar pathways to achieve the optimization aim. Equivalently to the energy constraint,

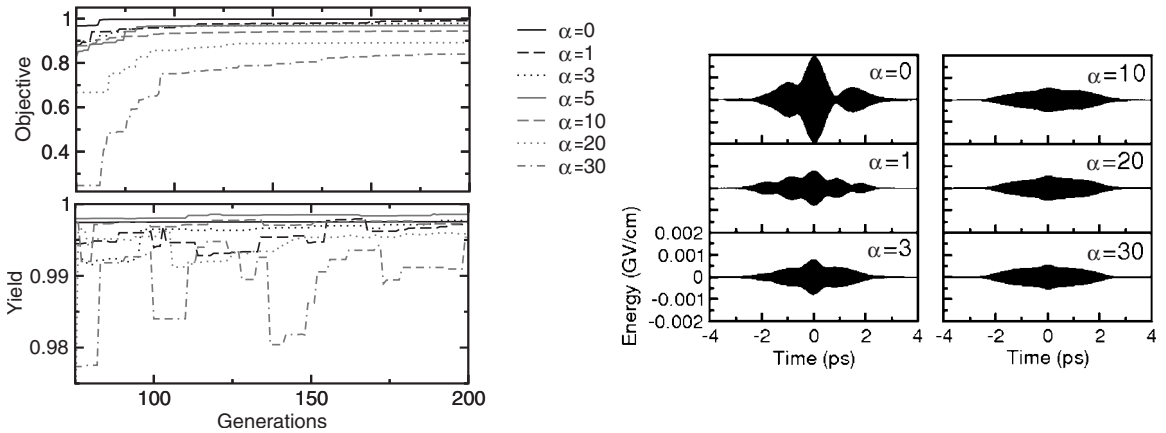

FIG. 3. Left: Convergence for different α-values; upper panel: objective; lower panel: yield. Right: Laser fields for different α values.

TABLE III. FL-pulse properties for analytic phase functions.

τ_p (fs)	E_0 (a.u.)	ω_c (cm^{-1})
212	0.001	1983

population in distinct vibrational levels (e.g., overtone states) or the complexity of the envelope can be constrained.

C. Pure phase modulation in analytic form

The exclusive application of analytic phase functions emerged from the aim to reduce the complexity of the shaped laser fields and to understand the underlying mechanisms [21]. In OCT, it is neither possible to address the phase function of the laser fields directly, nor can an analytic expression be defined. In the GA scheme this is straightforward to implement.

1. State-to-state transition in the T_{1u} mode of $W(CO)_6$

The control landscape for multipulses . We optimize the state-to-state transition $0 \rightarrow 1$ in the T_{1u} mode of $W(CO)_6$ with a sinusoidal phase modulation following the experiment [8].

$$\phi(\omega) = \sum_i a_i(\sin b_i\omega + c_i), \tag{1}$$

where we use $i=1$ and $c_i=0$. In analogy to the experiment, no transmittance function is employed. The FL-pulse properties are given in Table III.

The resulting multipulses are characterized by the phase parameters a_i and b_i. As a first step, we investigate the control landscape by scanning the influence of these parameters $a_1=a$ and $b_1=b$ on the quantum efficiency (Fig. 4), where a is dimensionless and b is a time, given in atomic units throughout the paper. Sections of the control landscape are shown in Fig. 4(a) for the large parameter range a: [0.6, 2.4] and b: [20 000, 40 000], the smaller inset is a zoom of the upper part. The surface is characterized by a high periodicity in b, with efficiencies ranging from 0% to 90%. The variation along a is significantly lower and thus b is the dominant control parameter.

The phase parameter a is the modulation depth, which determines the relative intensity of the single subpulses. The modulation time b defines the temporal shift between the individual subpulses. The temporal pattern of the carrier envelope phase (CEP) of the individual subpulses is constant for a given c value. For $c=0$ the CEP shift from subpulse to subpulse is π in the first half of the pulse sequence and zero in the second half [see Fig. 4(c), upper panel, dashed line]. This pattern is not affected by a variation of b. However, depending on b, an optical phase jump occurs between the subpulses, due to the combination of the fixed CEP pattern and the varying temporal shifts. The range of the optical phase jump $[0, 2\pi]$ corresponds to an oscillation period of the carrier frequency $\omega_c=1983$ cm^{-1} and is reflected in Fig. 4(a) in the periodicity of the control surface (a difference of

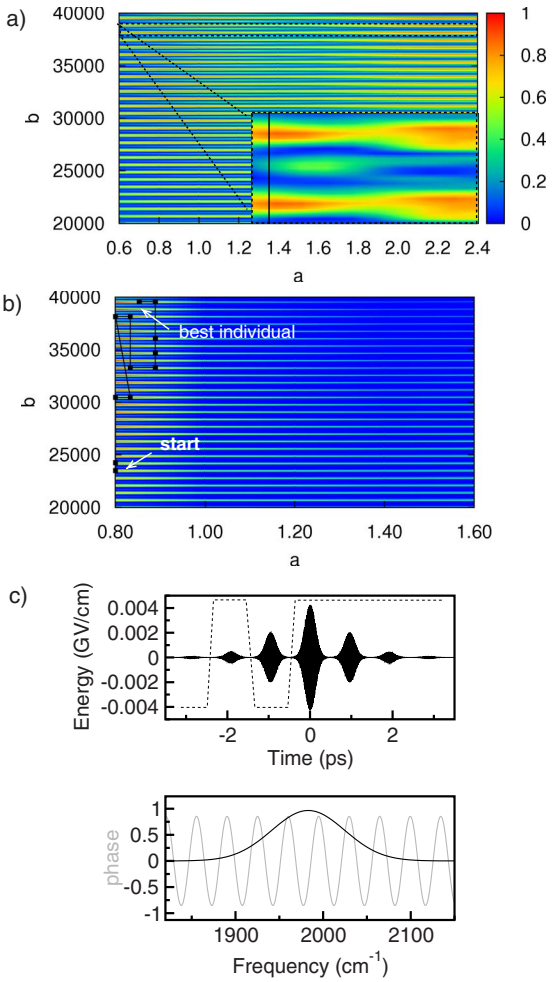

FIG. 4. (Color online) Control landscapes for the quantum yield as a function of the phase parameters a and b for the transition $0 \rightarrow 1$: (a) without constraints in the range a: [0.6, 2.4] and b: [20 000, 40 000] and detailed inset, (b) with constraints and best individuals of the GA run indicated, and (c) upper panel: best laser field with the CEP pattern; lower panel: spectrum (scaled, black line) and phase function (gray line).

$\Delta b \sim 700$ a.u. between the high-efficiency regions equals ~ 16.82 fs).

Mechanisms induced by multipulses.. The phase effects on the population transfer mechanism $|0\rangle \rightarrow |1\rangle$ are discussed exemplarily for a cut along the control surface marked in Fig. 4(a) by the vertical line in the smaller inset ($a=0.8$ and b: [38 000, 39 000]). In Fig. 5 the change in population of the states 0 [Fig. 5(a)] and 1 [Fig. 5(b)] are plotted as a function of time and b. For three b values ($b \sim 38\,200, 38\,550, 38\,900$) the initial state 0 is almost completely depopulated, but in only two cases ($b \sim 38\,200$ and $b \sim 38\,900$) the population is transferred into the target state 1. We select two values (marked as black arrows), one which leads to a high and one which leads to a low transfer efficiency into state 1. Their individual mechanisms are shown in Fig. 5(c). The corresponding laser fields are also included, as well as the optical phase jumps (in units of π) between the single subpulses. A b value of 38 900 induces a phase jump

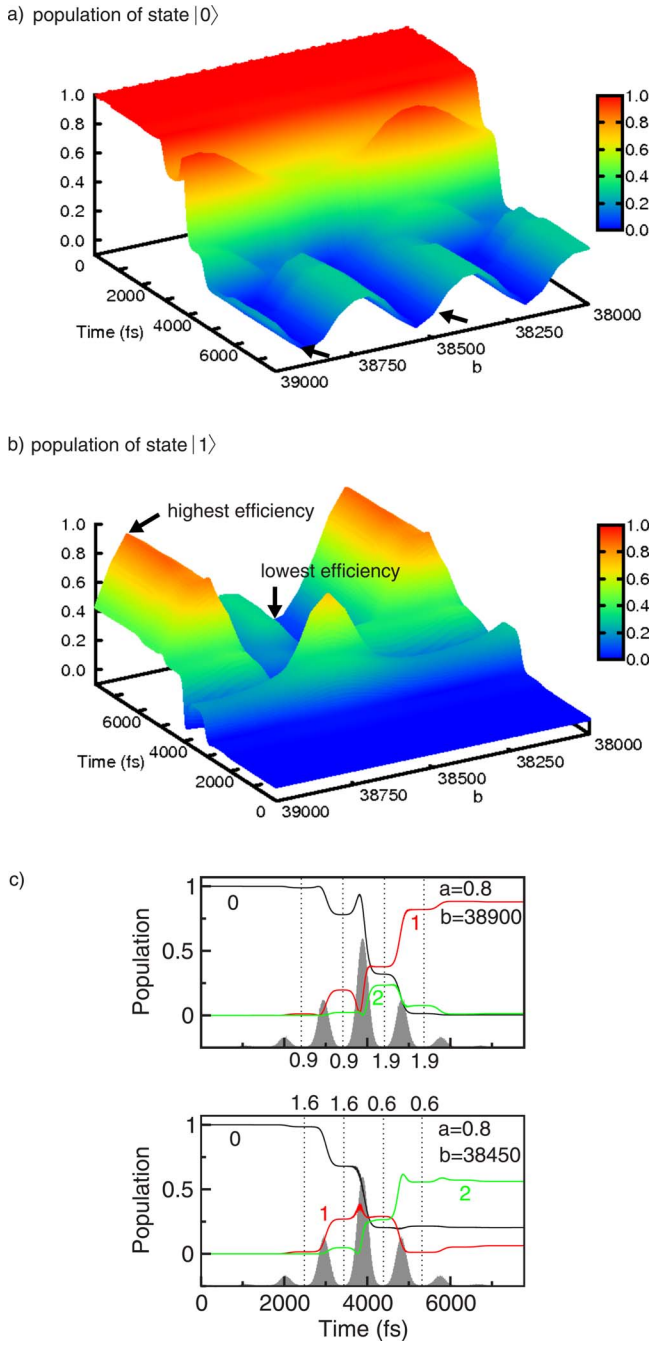

FIG. 5. (Color online) Population transfer mechanisms for the excitation $0 \rightarrow 1$ with the phase parameters $a=0.8$; b: [38 000, 39 000]. Progression of the population (a) in state 0 and (b) in state 1. The time axes point in opposite directions for better visibility. (c) Mechanisms, laser envelopes, and phase shifts for two selected sets of phase parameters.

of 1.9π. In the first half of the pulse sequence an optical phase jump of 0.9π results as the combination of the b induced phase jump and the CEP shifts from subpulse to subpulse. Since there are no CEP shifts in the second part, the optical phase jump is here 1.9π. From the transfer mechanisms [Fig. 5(c)], we can deduce that the first optical phase jumps of about π lead to subpulses, which reverse the action of the preceding pulse. See, e.g., the action of the subpulse at $t=3000$ fs or even more pronounced for $t=3900$ fs. This finding is general for all subpulses with optical phase jumps of π and is more effective, the closer the optical phase jump is to π. The optical phase jumps are most effective when the carrier frequency of the laser is in resonance with the transition energy. In the present study, the laser is tuned to the $0 \rightarrow 1$ transition, thus all overtone transitions (such as $1 \rightarrow 2$) are less affected.

The main subpulse [Fig. 5(c), upper panel] starts to depopulate the target state again. Due to the higher intensity, the target state is repopulated afterwards by the remaining pulse. For the next subpulse (second half of the pulse sequence), the optical phase jump is almost 2π and the population transfer into the vibrational state 1 is continued, whereas the overtone state 2 is depopulated. The same holds for the last subpulse. From the control landscape [Fig. 4(a)] and the mechanisms just discussed [Fig. 5(a)], we can conclude that the best results are reached for the given setting (i.e., molecular and FL-pulse properties) for optical phase jumps close to π in the first half of the pulse sequence and close to 2π in the second half. If $b=38\,450$ [Fig. 5(c), lower panel] optical phase jumps of 1.6π and 0.6π are obtained. In this case, neither a reversal of the excitation process, nor a continuation takes place. Instead, the net transfer in the first vibrational excited state is almost zero, while the overtone state is populated. Analogously, the complete control landscape depicted in Fig. 4(a) with respect to the periodicity in b can be understood. A deviation of its structure will only emerge when a parameter b is selected, which leads to subpulses overlapping in time.

Constraint on the pulse duration.. Variation of the parameter a determines the relative intensity of the single subpulses. Large a values increase the effective number of subpulses and equivalently the pulse duration. Such GA results would be unfavorable, when time limitation is required to protect the coherence of molecular processes. Therefore, we include a constraint within the objective function to confine the pulse duration as follows:

$$O = \frac{1}{N}\sum_{k=1}^{N} |\langle \Psi_{ik}(T)|\Phi_{fk}\rangle|^2 - \alpha_\tau \tau.$$

For τ we used the FWHM of the shaped pulse in atomic units and the penalty factor $\alpha_\tau = 0.000\,25$ [units $1/t$(a.u.)]. The structure of the control landscape changes [Fig. 4(b)] as the algorithm is forced to converge to a subspace with shorter durations. As can be traced from the GA run, the best result (88.4%) within the parameter range [0.0, 2.4] for a and [20 000, 40 000] for b is found after a few generations. The dots mark the best individuals of the generations and the line maps the GA search path on the landscape. The corresponding best laser field, its spectrum, and phase function are depicted in Fig. 4(c).

2. NOT gate in the T_{1u} mode of $W(CO)_6$

Starting with the FL pulse (Table III), suited for the fundamental state-to-state transition, we optimize a NOT gate

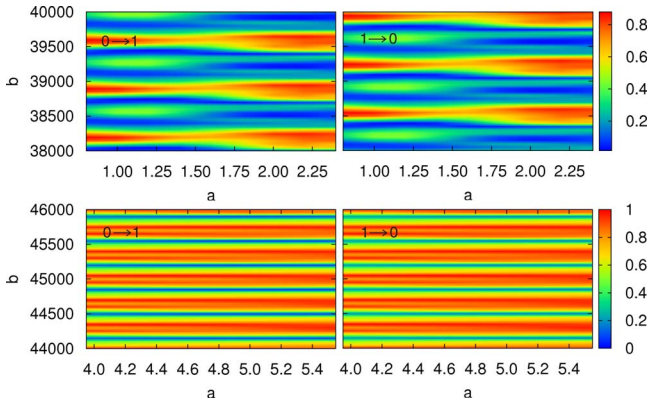

FIG. 6. (Color online) Control landscapes for the quantum yield as a function of the phase parameters a and b for both NOT processes $|0\rangle \rightarrow |1\rangle$ (left) and $|1\rangle \rightarrow |0\rangle$ (right). Upper panel: a, [0.8, 2.4]; b, [38000, 40000]. The periodicity of the surfaces is shifted by half an oscillation. Lower panels: a, [3.95, 5.55]; b, [44 000, 46 000]. The control landscapes for both switching processes match. The landscapes are evaluated for different FL pulses.

with a sinusoidal phase modulation and a slightly enlarged search space for b: [20 000, 50 000]. For this search space no high-fidelity solution of a NOT gate exists. The transition $|0\rangle \rightarrow |1\rangle$ can be switched with an efficiency of 81.8%, but the reverse process only reaches 48.2%. The explanation can be given from the control landscapes of both processes (Fig. 6). Their periodicity is shifted by half an oscillation, i.e., a maximum for a $|0\rangle \rightarrow |1\rangle$ transition matches a minimum or a secondary maximum condition for the $|1\rangle \rightarrow |0\rangle$ process and vice versa. The mechanism reveals that good solutions for the process $|0\rangle \rightarrow |1\rangle$ induce overtone transitions into state 2, when the laser field operates on state $|1\rangle$ to reverse the switching. The best efficiencies for the reverse process $|1\rangle \rightarrow |0\rangle$ are reached for a parameter $b \sim 38\,550$, where the optical phase jumps are $\sim 2\pi$ (1.86π) in the first part and $\sim \pi$ (0.86π) in the second part of the pulse sequence. The sequence of these optical phase jumps is exactly reversed to the progression required for the $|0\rangle \rightarrow |1\rangle$ transition. Consequently, unitary operations cannot be realized by a simple sinusoidal approach for the phase modulation; only when the distinct optical phase jumps are weakened can their implementation be successful. A straighforward solution is to increase the summation over $i > 1$ in Eq. (1). Thereby, the efficiency of the NOT gate can be raised to 95%, however, on the cost of higher complexity of the shaped laser fields. A new strategy is pursued to obtain efficient NOT gates with simple structures. Besides the phase parameters (a_i, b_i, c_i), we include the FL-pulse properties in the GA optimization simultaneously, which is related to amplitude shaping. Hence, we extend the genome of the GA by the carrier frequency ω_c, the maximum energy E_0, and the FWHM τ_p. This approach increases the flexibility of the GA optimization beyond the experimental possibilities and guarantees that the full dimensionality of the defined control parameter space can be used, here on the basis of sinusoidal phase modulation.

For the five degrees of freedom, we use the parameter ranges given in Table IV. As a result, a sinusoidal phase

TABLE IV. Parameter ranges for the FL-pulse properties and sinusoidal phase functions, for a NOT gate.

Parameter	Min.	Max.	GA result
a	0.0	5.0	4.75
b	20 000	60 000	44 625
E_0 (a.u.)	0.0	0.01	0.000 56
τ_p (fs)	0.0	2500	1504
ω_c (cm^{-1})	1950	2050	1990.9

modulated NOT gate could be optimized with an efficiency exceeding 99.6% [Fig. 7(a)]. The resulting parameters are given in Table IV and the control landscape of both NOT processes is depicted in Fig. 6, lower panel. Now, the maxima on the control surfaces of both processes $|0\rangle \rightarrow |1\rangle$ and $|1\rangle \rightarrow |0\rangle$ match. The significant change in the control landscapes (Fig. 6, upper and lower panels) arises from the combination of a rather narrow-band FL pulse and phase parameters, which lead to temporally overlapping subpulses now (Fig. 6, lower panel) without pronounced optical phase jumps. As a consequence, the multipulse character vanishes. The variation of amplitude in combination with phase modulation seems to be essential to realize a unitary transformation.

3. FL-pulse optimization for the state-to-state transition in the T_{1u} mode of $W(CO)_6$

The same optimization strategy is applied for the $0 \rightarrow 1$ state-to-state transition. The actual parameters are given in the Table V. The best result ($\sim 94\%$) within 200 generations for a population size of 50 is shown in Fig. 7(b). The optimal pulse is very similar in shape to the laser field found in the experiment [8]. The excitation mechanism also [Fig. 7(b), lower panel] provides the same features with the main part of population transferred by the second half of the multipulse. The explicit FL-pulse and phase properties are given in Table V.

This good agreement for the pulse structure and mechanism shows that our approach is able to match the search spaces in theory and experiment and we can predict that the

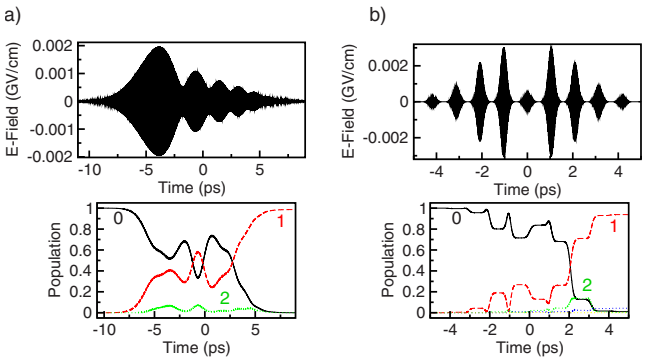

FIG. 7. (Color online) (a) GA optimized NOT gate and mechanism ($0 \rightarrow 1$ transition). (b) Optimized pulse for the $0 \rightarrow 1$ state-to-state transition in $W(CO)_6$ and mechanism.

TABLE V. Parameter ranges for the FL-pulse properties and sinusoidal phase functions, for a state-to-state transition.

Parameter	Min.	Max.	GA result
a	0.0	2.4	2.22
b	20 000	50 000	43 140
E_0 (a.u.)	0.0	0.01	0.001 07
τ_p (fs)	0.0	700	215.8
ω_c (cm^{-1})	1950	2000	1998.0

highest possible transition rate will be obtained for a FL pulse of 215.8 fs FWHM.

D. Prediction of GA quantum gates for $MnBr(CO)_5$

The GA optimization is extended to the two-qubit system $MnBr(CO)_5$, for which we previously [20] optimized a universal set of quantum gates with OCT. The predicted, highly efficient quantum gates were simple structured and we are now interested, whether comparable solutions can be provided by the GA.

We optimize a universal set of quantum gates, with great importance attached to structural simplicity, as a benchmark for future experimental searches. A universal set of quantum gates consists of a CNOT, NOT, Π, and Hadamard gate. We optimize the gates involving population transfer (CNOT, NOT, and Hadamard) explicitly and assume that the Π gate is implemented after a Hadamard transformation by a delay, which induces the correct phase rotation. Quantum gates, yielding phase correct target states, can be optimized by maximizing the fidelity, defined as

$$F = \frac{1}{N^2}\left|\sum_{k}^{N}\langle\Psi_{ik}|\Phi_{fk}(T)\rangle\right|^2.$$

Alternatively, one can optimize the population transfer only,

$$P = \frac{1}{N}\sum_{k=1}^{N}|\langle\Psi_{ik}(T)|\Phi_{fk}\rangle|^2,$$

and make use of the free phase evolution of the qubit basis states, i.e., append a phase gate. This is equivalent to a certain delay time of several femto-to picoseconds, in which the phase of each state evolves until the correct phase relation is reached at the end of the delay [22]. The second approach converges faster and corresponds to the direct, experimental observable. Exemplarily, the CNOT and NOT gates are depicted in Fig. 8, where the subscript E denotes the gate is operating on the E symmetric mode and A on the A_1 symmetric mode, respectively. These gates were optimized by maximizing the population transfer. A delay time has to be attached to receive the correct phase relation. We used 15 pixels with a spectral width of 5 cm^{-1} for each pixel, the phase variation was confined to $[0,2\pi]\times 0.5$, and no further constraints were applied. The quantum gates operate very efficiently with a population transfer exceeding at least 99.0%. They are similar, simple structured compared to the OCT results [20], but clearly longer in duration as the defined phase space is again fully utilized, allowing for large amplitude modulations of the mask functions. In OCT calculations, the phase function cannot be addressed directly, however, the penalty factor together with the choice of the total laser interaction time can suppress unnecessary jumps in phase and/or transmittance.

For the $CNOT_E$ gate, we also maximize the fidelity of the process using a GA. We determine the duration of the shaped pulse using a threshold value of 5×10^{-6} a.u. of the electric field. The propagation starts when this threshold is exceeded the first time. Equivalently, it ends when the value is reached the last time. At this final time, the fidelity of the whole process is calculated. In Fig. 9(a), a comparison of the convergence of both approaches, the maximization of the fidelity versus the population transfer, is shown. We used a population size of 50 and 1000 generations. The GA run for the pure population transfer (gray line) reaches an efficiency over 99% after approximately 100 generation. The optimal

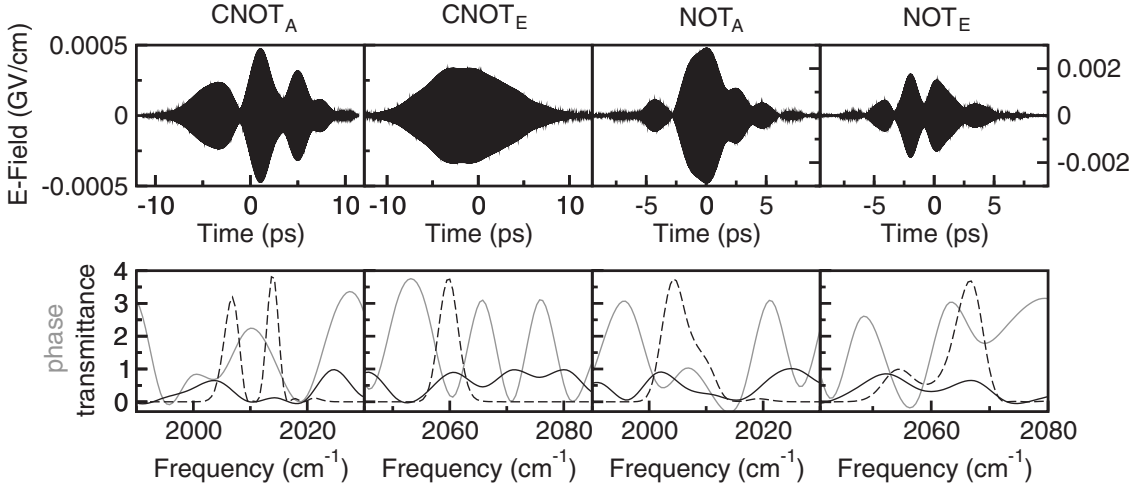

FIG. 8. GA optimized CNOT and NOT gates for $MnBr(CO)_5$, operating either on the A, or on the E mode, with spectra (dashed, black lines), phase functions (solid, gray lines), and transmittance functions (solid, black lines) depicted in the lower panels.

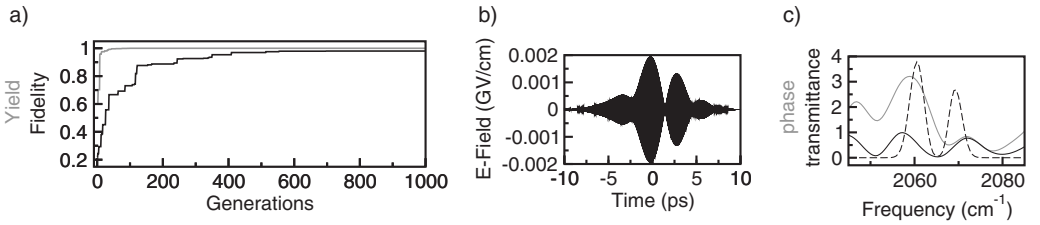

FIG. 9. (a) Convergence of the maximization of the population transfer versus the fidelity for the CNOT_E gate. Phase-correlated optimization of the CNOT gate: (b) Laser field. (c) Spectrum (scaled, dashed, black line), phase (gray line), and transmittance function (solid, black line).

quantum gate is depicted in Fig. 8. An additional delay time of ~4 ps makes the CNOT gate phase correct for use in quantum algorithms. In the second case [Fig. 9(a), black line], a maximum fidelity of ~97% is reached after 700 generations. The slightly reduced fidelity is mainly due to an incomplete population transfer.

Additionally, we tested the implementation prospects of pure sinusoidal phase modulation of two-qubit quantum gates. In the multipulse parameter ranges, the efficiencies of the quantum gates cannot compete with free phase and amplitude modulated laser fields. Thus, for the experimental implementation of multiqubit quantum gates, we propose the more flexible approach of a pixeled mask function. To avoid unnecessary complex pulse structures, we suggest confining the codomain of the phase to a limited range.

V. CONCLUSION

In this paper, we discussed the differences originating from the control in the frequency domain by a GA and in the time domain by OCT. With OCT, it was always possible to find the simplest structured laser fields for high-fidelity solutions, which are probably most robust. By default, a GA is used in closed-loop experiments and its theoretical simulation allows for reliable predictions in the search space, strictly limited to the experimental parameters and their variation range. Pixel-based mask functions often lead to complex pulse structures. In the GA search, we introduced approaches to decrease the complexity of the resulting pulse structures, borrowing concepts from our previous OCT work. Our objectives were state-to-state transitions and unitary transformations in the vibrational manifold of transition metal carbonyls. For pixeled phase and transmittance functions, we showed that longer FL pulses, as well as the restriction of the codomain of the phase function leads to simplifications of the pulse envelopes. Additionally, we implemented constraints in the GA, which can be used to reduce the field intensity or the pulse duration and guide the GA runs into distinct subspaces of simple structured results. Analogously, constraints may be included, which decrease the complexity of the envelope function or the degree of the overtone excitation. For constrained GA runs, we could find for both objectives solutions approaching the subspace of optimal OCT results.

We also investigated the effect of sinusoidal phase modulation, frequently used in experiment, omitting amplitude modulation. We calculated the corresponding control landscape and from its analysis, we derived the physical mechanism of the vibrational multipulse excitation. The laser fields and transfer mechanism obtained for the state-to-state transfer in $W(CO)_6$ agrees very well with the experiment [8]. The best, highly efficient solutions were obtained when the FL-pulse properties (carrier frequency, maximum energy, and FWHM) were optimized simultaneously. From our results, we can predict that multipulses are not suitable for the implementation of unitary transformations. This could easily be explained by the analysis of the control landscapes. When the sinusoidal phase approach is used, an optimized FL pulse is essential for high fidelities, i.e., a certain amount of amplitude shaping is required. In general, we found that pixeled phase and transmittance functions will lead to higher quantum yields. To reduce the complexity of the resulting field envelope, alternatively to the analytic phase confinement, parameter constraints and limits on the codomains can be introduced, without loss of flexibility.

In summary, with the GA optimization scheme, we have the possibility to explore the experimental search space by setting all relevant parameters to the actual, experimental conditions. The comparison showed that we reached good agreement for pulse shapes and mechanisms. Stimulated by these results, we introduced successfully several constraints to approach the subspace of low-complexity OCT results and propose simple structured, robust pulses for the GA search with high efficiencies. For the experimental implementation of unitary transformations based on vibrational qubits, we can predict that the use of pixeled phase and amplitude modulation together with a careful choice of constraints will be most promising.

ACKNOWLEDGMENT

The authors would like to thank the Deutsche Forschungsgemeinschaft for financial support through the Normalverfahren and through the excellence cluster "Munich Center for Advanced Photonics" (MAP).

[1] W. Zhu, J. Botina, and H. Rabitz, J. Chem. Phys. **108**, 1953 (1998).
[2] W. Zhu and H. Rabitz, J. Chem. Phys. **109**, 385 (1998).
[3] D. Tannor and S. A. Rice, J. Chem. Phys. **83**, 5013 (1985).
[4] A. Assion, T. Baumert, M. Bergt, T. Brixner, B. Kiefer, V. Seyfried, M. Strehle, and G. Gerber, Science **282**, 5390 (1998).
[5] P. Nuernberger, G. Vogt, T. Brixner, and G. Gerber, Phys. Chem. Chem. Phys. **9**, 2470 (2007).
[6] C. M. Tesch and R. de Vivie-Riedle, Phys. Rev. Lett. **89**, 157901 (2002).
[7] C. Gollub, M. Kowalewski, and R. de Vivie-Riedle, Phys. Rev. Lett. **101**, 073002 (2008).
[8] D. B. Strasfeld, S. H. Shim, and M. T. Zanni, Phys. Rev. Lett. **99**, 038102 (2007).
[9] B. M. R. Korff, U. Troppmann, K.-L. Kompa, and R. de Vivie-Riedle, J. Chem. Phys. **123**, 244509 (2005).
[10] T. Witte, J. S. Yeston, M. Motzkus, E. J. Heilweil, and K.-L. Kompa, Chem. Phys. Lett. **392**, 156 (2004).
[11] M. Tsubouchi and T. Momose, Phys. Rev. A **77**, 052326 (2008).
[12] D. Weidinger and M. Gruebele, Mol. Phys. **105**, 13–14 (2007).
[13] M. J. Frisch, G. W. Trucks, H. B. Schlegel, G. E. Scuseria, M. A. Robb, J. R. Cheeseman, J. A. Montgomery, T. Vreven, K. N. Kudin, J. C. Burant, K. Raghavachari, J. M. Millam, S. S. Iyengar, J. Tomasi, V. Barone, B. Mennucci, M. Cossi, G. Scalmani, N. Rega, G. A. Petersson, H. Nakatsuji, M. Hada, M. Ehara, K. Toyota, R. Fukuda, J. Hasegawa, M. Ishida, T. Nakajima, Y. Honda, O. Kitao, M. Nakai, M. Klene, X. Li, J. E. Knox, H. P. Hratchian, J. B. Cross, C. Adamo, J. Jaramillo, R. Gomperts, R. E. Stratmann, O. Yazyev, A. J. Austin, R. Cammi, C. Pomelli, J. W. Ochterski, P. Y. Ayala, K. Morokuma, G. A. Voth, P. Salvador, J. J. Dannenberg, V. G. Zakrzewski, S. Dapprich, A. D. Daniels, M. C. Strain, O. Farkas, D. K. Malick, A. D. Rabuck, K. Raghavachari, J. B. Foresman, J. V. Ortiz, Q. Cui, A. G. Baboul, S. Clifford, J. Cioslowski, B. B. Stefanov, G. Liu, A. Liashenko, P. Piskorz, I. Komaromi, R. L. Martin, D. J. Fox, T. Keith, M. A. Al-Laham, C. Y. Peng, A. Nanayakkara, M. Challacombe, P. M. W. Gill, B. Johnson, W. Chen, M. W. Wong, C. Gonzalez, and J. A. Pople, GAUSSIAN'03 (Gaussian, Inc., Pittsburgh, PA, 2003).
[14] J. Manz, K. Sundermann, and R. de Vivie-Riedle, Chem. Phys. Lett. **290**, 415 (1998).
[15] D. Zeidler, S. Frey, K.-L. Kompa, and M. Motzkus, Phys. Rev. A **64**, 023420 (2001).
[16] D. E. Goldberg, *Genetic Algorithms in Search, Optimization, and Machine Learning* (Addison-Wesley, Reading, MA, 2005).
[17] GAlib genetic algorithm package, Matthew Wall, Massachusetts Institute of Technology.
[18] T. Hornung, M. Motzkus, and R. de Vivie-Riedle, J. Chem. Phys. **115**, 3105 (2001).
[19] M. Ndong, D. Lauvergnat, X. Chapuisat, and M. Desouter-Lecomte, J. Chem. Phys. **126**, 244505 (2007).
[20] B. M. R. Schneider, C. Gollub, K.-L. Kompa, and R. de Vivie-Riedle, Chem. Phys. **338**, 2–3 (2007).
[21] J. Herek, W. Wohlleben, R. J. Cogdell, D. Zeidler, and M. Motzkus, Nature (London) **417**, 533 (2002).
[22] U. Troppmann, C. Gollub, and R. de Vivie-Riedle, New J. Phys. **8**, 100 (2006).